Numerical and experimental analysis of complex surface acoustic wave fields

M. Streibl, H.-J. Kutschera, W. Sauer, Achim Wixforth

Angaben zur Veröffentlichung / Publication details:

Streibl, M., H.-J. Kutschera, W. Sauer, and Achim Wixforth. 2000. "Numerical and experimental analysis of complex surface acoustic wave fields." In *IEEE Ultrasonics Symposium Proceedings: An International Symposium, 22 - 25 October 2000, San Juan, Puerto Rico, USA*, 205–8. Piscataway, NJ: IEEE. https://doi.org/10.1109/ultsym.2000.922540.

Numerical and Experimental Analysis of Complex Surface Acoustic Wave Fields

M. Streibl, H.-J. Kutschera*, W. Sauer and A. Wixforth

Sektion Physik der Ludwig Maximilians Universität and CeNS,

Geschwister-Scholl-Platz 1, 80539 München, Germany

Abstract— Sophisticated high frequency signal processing as well as sensor applications based on surface acoustic waves (SAW) often require a complex transducer layout. We present a simple numerical technique based on a Huygens-type construction to calculate acoustic wave fields for a arbitrary given transducer layout. Approximating the slowness curve of different substrate materials by a parabolic function, we calculate the SAW far field with superposition of circular waves emitted by distributed point sources. Our numerical results for different transducer geometries are in excellent agreement with measurements of the acoustic wave field by an X-ray topographic technique.

I. Introduction

For new applications, especially for scientific purposes, there is often the need for complex transducer geometries to get exceptional SAW fields. For instance, as has been recently demonstrated [1], spatially resolving on-chip sensor elements can be realized using so-called tapered transducers [2] usually used for bandpass applications. The finger period in these special transducers changes linearly over the transducer aperture. For a fixed frequency an acoustic wave is only launched in a small stripe of the transducer where the resonance condition is matched. The tapered transducer, hence, allows for the excitation of a very narrow SAW beam and an adjustability of the lateral beam position within the transducer aperture. The SAW beam can interact with locally induced stress or charge carriers. The spatial resolution for these sensors strongly depends on the width and the intensity of the wave field. Focusing SAWs for waveguide coupling applications requires also a detailed knowledge of the SAW field. Therefore it is beneficial to have a simple and fast numerical technique to calculate the wave field for a given arbitrary transducer geometry.

*e-mail: hans-joerg.kutschera@physik.uni-muenchen.de

An often used technique to calculate necessary transducer geometries for arbitrary wanted wave field in anisotropic materials was first introduced by Kharusi and Farnell [3] and is called the Angular Spectrum of Plane Wave method. Starting point is a scalar source distribution that describes, e.g., the electric potential or the z-amplitude of the desired wave field. By doing a Fourier transformation this distribution is decomposed into plane waves. The anisotropy of the crystal is considered in terms of the wave vector dependency on the slowness curve $k(\theta) = 2\pi f/v(\theta)$. The plane waves are then superimposed and to get the initially wanted wave field the transducer fingers have to be patterned along the phase fronts of the resulting wave field. This method needs a lot of computing power, especially if the complete anisotropy is taken into account. As mentioned above it is necessary to have the possibility for a fast evaluation of the wave field for a given arbitrary transducer geometry. For this purpose we introduce in the next section a simple method that is based on an inverse approach similar to the Huygens principal in optics. Experimentally, the SAW fields generated by given transducers can be monitored by various techniques, like scanning acoustic force microscopy [4] and optical deflection [5]. In the third section we present some new results obtained by a X-Ray topographic technique [6] and compare them with our numeric results.

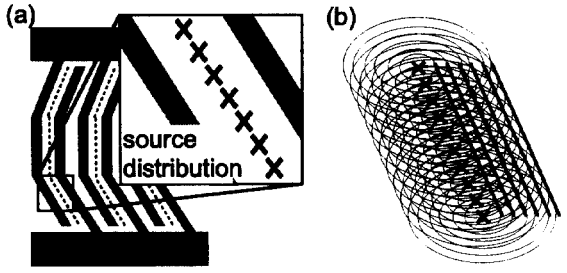

Fig. 1. Model to calculate the acoustic wave field similar to the Huygens principal of optics: (a) Positioning of source points along lines of equal potential. (b) Superposition of propagating plane waves considering the anisotropy of the crystal.

II. Numerical Model

The starting point of our numerical approach is similar to the Huygens principal in optics. First one arranges source points on lines of constant potential, i.e. along the transducer fingers (Fig. 1). Every point represents a source of a plane wave $exp[i(\mathbf{kr}-\omega t)]$, where $k = k(\theta) = 2\pi f/v_{SAW}(\theta)$ and θ is the angle between the vector $\mathbf{r}$ and the main propagation direction — in the case of GaAs the [110]-direction. The amplitude A of the SAW at an arbitrary point (x,y) arises from the superposition of all plane waves:

$$A(x,y) = \sum_{i=0}^{N}\sum_{j=0}^{M} exp[i(\mathbf{kr}-\omega t)], \qquad (1)$$

with

$$\mathbf{r} = (x - x_{ij}, y - y_{ij}), \qquad (2)$$

where x_{ij} and y_{ij} are the coordinates of the j-th source points in the i-th period of the transducer. The intensity $I(x,y)$ of the wave is then given by

$$I(x,y) = \sqrt{A(x,y)\cdot A^*(x,y)}. \qquad (3)$$

Far away from the transducer θ is small and one can use a parabolic approximation for v_{SAW} to accelerate the numeric calculation.

$$v(\theta) = v_0(1-\gamma\theta^2), \qquad (4)$$

In our examples we use the anisotropy parameter γ for GaAs, which is equal to $0.455\,rad^{-2}$ [7].

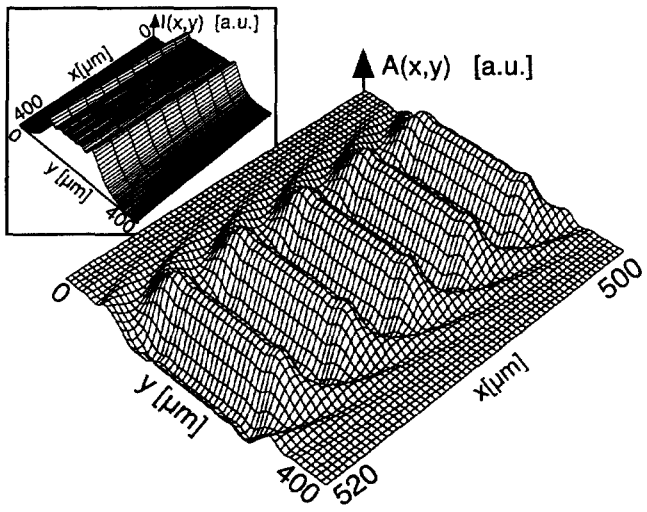

Fig. 2. Numerical result for the wave field of a normal split-1 transducer. (a) is an 400 × 400 µm²–overview of the intensity, while (b) is a enlarged 20 × 400 µm² view of the amplitude.

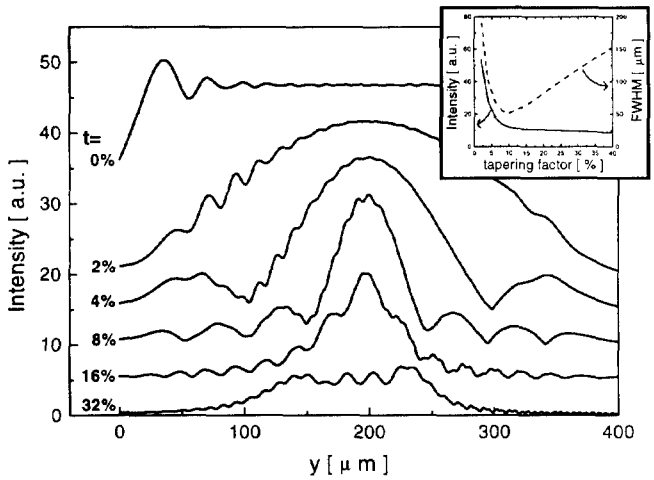

Fig. 3. Intensity profile of the wave field generated by a tapered transducer operated at the center frequency after 500 µm propagation for different tapering factors. The different curves are offseted by 5 for clarity. The inset shows the FWHM (—) and the integrated value (- -) of the intensity in main SAW path in dependence of the tapering factor.

The described algorithm was implemented in a C++ routine. Typical parameters to simulate the source, i.e. the transducer geometry, are N=100 periods with M=100-200 source points per period. The number of calculated points of the wave field $K \times L$ has been usual $K, L = 50...100$. Taking into account the double summation the loop has to be repeated $2.5\cdot 10^7 ... 4\cdot 10^8$ times to calculate the wave field. After all, the simplicity of the calculation allows a high speed computation, so that typical running times on a modern computer are below 10 minutes.

To demonstrate the program's performance, we will discuss two examples. At first the numerical result for the wave field of a normal split-1 transducer with aperture of 200 µm and finger period of 4 µm is plotted in Fig. 2. The inset of Fig. 2 gives an overview ($400 \times 400\,\mu m^2$) of the wave field intensity in the SAW path. Because of diffraction at the finite transducer aperture, one clearly recognizes the increase of amplitude at the edges of the SAW path. In a more detailed view the amplitude shows a definite phase shift at the border of the SAW path.

As a second example we discuss the wave field generated by a tapered transducer with focus on the above mentioned sensor application. The numerical calculation was done for a transducer with an aperture of 400 µm and a maximum period of 4 µm. The transducer is operated at its center frequency. The wave field intensity 500 µm away from the transducer is plotted in Fig. 3 for different tapering factors t. For

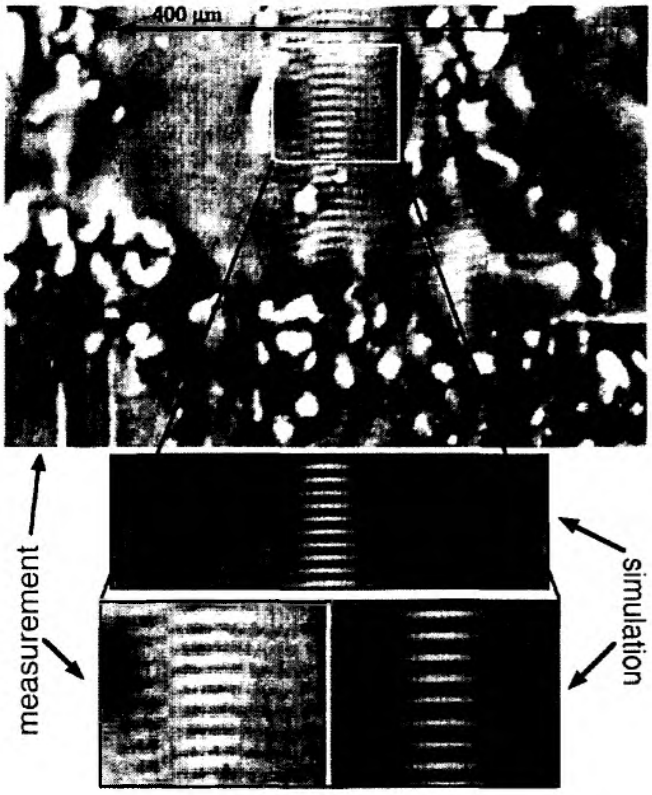

Fig. 4. Comparison of the X-ray topographic imaging result of the wave field generated by a tapered transducer with the numeric simulation.

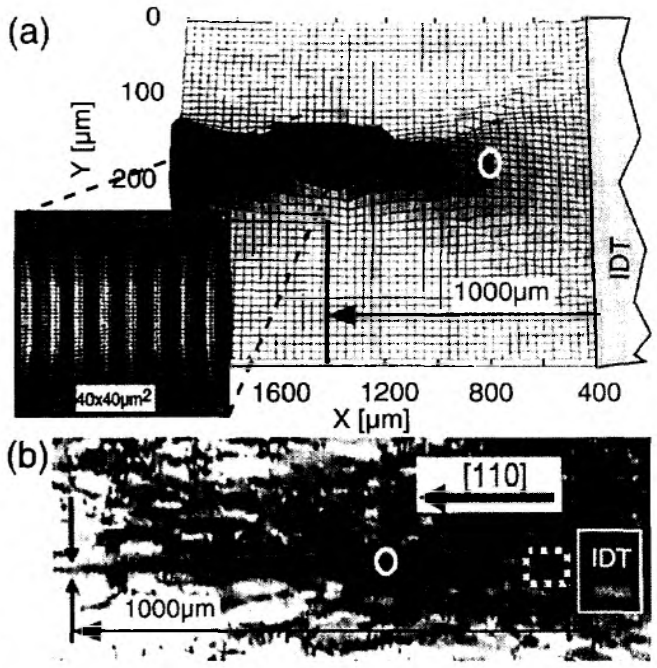

Fig. 5. (a) Numerical and (b) experimental results of the wave field of a focusing transducer. The inset of (a) resembles the expansion of the focal point, which is due to the anisotropy of the crystal.

small tapering factors the SAW intensity along the aperture is smooth and the acoustic wave propagates basically along the whole aperture. With increasing t the intensity distribution more and more resembles the expected sinc-function and the width of the main SAW decreases, until for very high t diffraction gets more and more important and the overall intensity decreases and broadens again.

The inset of Fig. 3 summarizes these facts, where the FWHM and the integrated intensity of the SAW main path are plotted. The intensity decreases continously with increasing tapering factor, as only a small section of the transducer is driven resonantly for a certain excitation frequency. In contrast the FWHM shows a clear minimum at $t \approx 10\%$. This has to be considered for the design of sensor elements, since the width of the SAW path for a certain excitation frequency determines the lateral resolution, while the intensity is important for the magnitude of the signal.

III. Comparison to experimental results

A powerful method to visualize acoustic wave fields is given by X-ray topographic imaging. Short synchrotron X-ray pulses are reflected by the surface under the Bragg angle. The repetition frequency of the pulses is multiplied with a constant factor by a phase locked loop, amplified, and used as excitation frequency for the SAW device. Therefore the surface wave is always in phase to the light pulses and one stroboscopically obtains a standing image of the propagating wave. A more detailed description can be found in [6]. Typical measurements are shown in Fig. 4 and 5(b). Apart from the SAW-induced contrast variation, the typical defect structure of the substrate becomes visible.

A. Wave field of a tapered transducer

The described method can now be used to compare the numerical results with the measured wave field. As first example serves the wave field generated by a tapered transducer (Fig. 4). In this case the transducer has a maximum period of $\lambda_{max} = 5\,\mu m$, an aperture of 400 µm and the tapering factor is 10%. In the left and right lower corner of the overview picture the contact pads of the transducer being aligned to the

aperture can be identified. The measurement shows the expected narrow SAW path and one also recognizes a broadening of the SAW path in the propagation direction. The experimental results are in total agreement with the numerical solution. This is illustrated by the detailed view of Fig. 4 where not only the width of the SAW path, but also the side maxima with the characteristic phase shift compared to the main path are well reproduced. In this context, it should be mentioned that there is no free parameter in the calculation. The position of the SAW path is directly given by the excitation frequency that is put into the source distribution (eq. 1).

B. Wave field of focusing transducers

The final example is summarized in Fig. 5 and shows the numeric calculation of the wave field of a focusing transducer in comparison to the experiment. The transducer is built from segments of a circle and has a aperture of 400 µm, a period of 5 µm, and the number of finger pairs is $N = 80$. The white circles indicate the nominal focal distance, i.e. the distance where the wave would have been focused, if the anisotropy of the crystal is not considered. The calculation shows that the actual focal distance is 600 µm behind the nominal focal distance. This and the fact that through the anisotropy of the crystal the focal point is expanded along the propagation direction is well confirmed by the X-ray topographic measurements.

IV. Conclusion

All these examples yield to important qualitative and quantitative statements about acoustic wave fields. Furthermore it could be shown that the numerical results are in good agreement with experimental results. Therefore the introduced numerical method proves valuable for a fast evaluation of complex wave fields, the design of complex transducer geometries, as well as to describe measurement results.

Acknowledgment

The authors gratefully acknowledge fruitful discussions with L. Reindl, W. Ruile, and J. P. Kotthaus, and financial support by the Deutsche Forschungsgemeinschaft (DFG) and the Volkswagen Stiftung.

References

[1] M. Streibl, A. Wixforth, J. P. Kotthaus, A. O. Govorov, C. Kadow, A. C. Gossard, *Imaging of acoustic charge transport in semiconductor heterostructures by surface acoustic waves*, Appl. Phys. Lett. **75**, 4139 (1999)

[2] L. Solie, *Tapered Transducers - Design and Application*, IEEE Intl. Ultrason. Symp. pp. 1-11 (1998)

[3] M. S. Kharusi and G. W. Farnell, *Diffraction and Beam Steering for Surface-Wave Comb Structures on Anisotropic Substrates*, IEEE Trans. **SU-18**, 34 (1971)

[4] E. Chilla, T. Hesjedal, H.-J. Fröhlich, *Nanoscale determination of phase velocity by scanning acoustic force microscopy*, Phys. Rev. B **55**, 15852 (1997)

[5] P. V. Santos, *Acoustic field mapping on GaAs using microscopic reflectance and reflectance anisotropy*, Appl. Phys. Lett. **74**, 4002 (1999)

[6] W. Sauer, M. Streibl, T. H. Metzger, A. Haubrich, S. Manus, A. Wixforth, J. Peisl, A. Mazuelas, J. Hartwig, J. Baruchel, *X-ray imaging and diffraction from surface phonons on GaAs*, Appl. Phys. Lett. **75**, 1709 (1999)

[7] W. D. Hunt, Y. Kim, F. M. Fliegel, *A synopsis of surface acoustic wave propagation on* {100}- *cut* ⟨110⟩- *propagating gallium arsenide*, J. Appl. Phys. **69**, 1936 (1991)